The Astrophysical Journal, 782:39 (8pp), 2014 February 10 doi:10.1088/0004-637X/782/1/39

THE DYNAMICAL FINGERPRINT OF CORE SCOURING IN MASSIVE ELLIPTICAL GALAXIES

J. Thomas[1,2], R. P. Saglia[1,2], R. Bender[1,2], P. Erwin[1,2], and M. Fabricius[1,2]
[1] Max Planck-Institute for extraterrestrial Physics, P.O. Box 1312, Giessenbachstr. 1, D-85741 Garching, Germany; jthomas@mpe.mpg.de
[2] Universitätssternwarte München, Scheinerstraße 1, D-81679 München, Germany
Received 2013 November 14; accepted 2013 December 20; published 2014 January 24

ABSTRACT

The most massive elliptical galaxies have low-density centers or cores that differ dramatically from the high-density centers of less massive ellipticals and bulges of disk galaxies. These cores have been interpreted as the result of mergers of supermassive black hole binaries, which depopulate galaxy centers by gravitationally slingshotting central stars toward large radii. Such binaries naturally form in mergers of luminous galaxies. Here, we analyze the population of central stellar orbits in 11 massive elliptical galaxies that we observed with the integral field spectrograph SINFONI at the European Southern Observatory Very Large Telescope. Our dynamical analysis is orbit-based and includes the effects of a central black hole, the mass distribution of the stars, and a dark matter halo. We show that the use of integral field kinematics and the inclusion of dark matter is important to conclude on the distribution of stellar orbits in galaxy centers. Six of our galaxies are core galaxies. In these six galaxies, but not in the galaxies without cores, we detect a coherent lack of stars on radial orbits in the core region and a uniform excess of radial orbits outside of it: when scaled by the core radius r_b, the radial profiles of the classical anisotropy parameter $\beta(r)$ are nearly identical in core galaxies. Moreover, they quantitatively match the predictions of black hole binary simulations, providing the first convincing dynamical evidence for core scouring in the most massive elliptical galaxies.

Key words: galaxies: elliptical and lenticular, cD – galaxies: evolution – galaxies: kinematics and dynamics – galaxies: structure

1. INTRODUCTION

Elliptical galaxies have long been believed to be the end-product of collisions, or mergers, between galaxies. Tracing back in time the evolutionary history of individual ellipticals is difficult, however, since galaxy collisions involve strong distortions in the gravitational potential that randomize the distribution of stellar orbits. Most of the information about the structure of possible progenitor galaxies and even the number of mergers is therefore erased. For example, over several orders of magnitude in radius, the smooth light profiles of elliptical galaxies can be well described by the single three-parameter Sérsic function (Sérsic 1963; Caon et al. 1993). However, the most massive galaxies often exhibit surface brightness profiles that are, interior to a "break" or "core" radius r_b, significantly flatter than the inward extrapolation of the outer, Sérsic-like profile. The resulting cores have typical sizes of $r_b \sim 50$–500 pc. Cores are not the only characteristic by which the most massive and brightest ellipticals are distinct from fainter elliptical galaxies: massive ellipticals are less flattened, with boxy instead of disky isophotes, and are dominated by unordered, rather than rotational, stellar motions (e.g., Kormendy & Bender 1996; Faber et al. 1997). Based on statistical comparisons between observed galaxies and numerical *N*-body simulations, these morphological differences provide circumstantial evidence for two distinct formation paths. Fainter ellipticals likely form from mergers of disk-dominated progenitor galaxies that are rich in gas; the gas can then settle into a rotational, disky configuration before forming new stars. The most massive ellipticals, however, are thought to form through gas-poor (i.e., elliptical–elliptical) mergers.

The existence of cores represents a challenge to our understanding of the merging process. The central structure of a merger without gas is dominated by the more concentrated of the two progenitors: the steeper central density cusp survives (Fulton & Barnes 2001; Boylan-Kolchin & Ma 2004). Since high-mass ellipticals are thought to be built from mergers of lower-mass ellipticals, which have steep central-density cusps, the shallower cores in more massive ellipticals have to be the result of another physical mechanism. Supermassive black holes (SMBHs) that reside in the centers of essentially all elliptical galaxies provide such a core formation mechanism: during a merger, the two central SMBHs of the progenitors sink to the center of the remnant by dynamical friction and form a binary. The binary then loses angular momentum to stars in the center via three-body interactions, scouring out the core while becoming progressively more tightly bound until it eventually merges (Begelman et al. 1980).

Although this model currently represents the only convincing scenario for core formation, only indirect evidence for this process had been presented previously: the size of the core and the amount of starlight that is "missing" in the centers of core galaxies have been found to scale approximately with the mass of the central black hole, as predicted by theory (Graham 2004; Kormendy & Bender 2009; Kormendy & Ho 2013). By their very nature, however, missing-light measurements depend strongly on model-dependent assumptions about the original central light profiles (Hopkins & Hernquist 2010).

Core scouring by a black hole binary proceeds after the phase of violent randomization of stellar orbits by a merger. This is crucial because stellar orbits then become an important "archaeological" diagnostic for core formation. The two-body relaxation time for stars in galaxies exceeds the age of the universe. Galaxies are therefore collisionless systems and once the stars have settled on their orbits, the phase-space distribution remains conserved for very long times. Core scouring changes the orbit distribution: only radial orbits allow for close passage past the galaxy center and thus only stars on radial orbits can reach the vicinity of the central binary black hole and get ejected. Consequently, the orbital structure left behind in the core after core scouring is predicted to be strongly biased in favor of tangential orbits, while the ejected stars contribute to enhanced

radial motions outside the core (Quinlan & Hernquist 1997; Milosavljević & Merritt 2001).

That stellar orbits around black holes are predominantly tangential is predicted not only by SMBH-binary models. The traditional picture for the formation of non-core galaxies through gas-rich mergers leads to an enhanced population of tangential orbits as well because the new stars that form from gas that falls in during/after the merger are likely to end up in a rotating structure that is supported by near-circular orbits. Likewise, the changes in the gravitational potential induced by an (adiabatically) growing black hole that is fed by gas reshape stellar orbits toward becoming more tangential as well (Young 1980; Goodman & Binney 1984; Quinlan et al. 1995).

Previous dynamical studies addressing the distribution of stellar orbits in the vicinity of SMBHs focused mainly on the mere detection of tangential orbits, but did not try a direct comparison with predictions from theoretical models. This is necessary, however, to distinguish between dissipational and dissipationless core formation, since both predict stars to predominantly move along tangential orbits.

Early dynamical models, in addition, lacked dark matter (DM) halos (Cretton & van den Bosch 1999; Gebhardt et al. 2000, 2003, 2007; Verolme et al. 2002; Shapiro et al. 2006; Houghton et al. 2006; Nowak et al. 2008; Cappellari et al. 2009; Siopis et al. 2009; Gültekin et al. 2009; Krajnović et al. 2009; van den Bosch & de Zeeuw 2010). Omission of DM leads to a bias in the masses of the stars and the central black hole (Gebhardt & Thomas 2009; Rusli et al. 2013b). Distributions of stellar orbits measured without including the effect of DM are correspondingly unreliable.

For about half of the ∼ two dozen galaxies that have been modeled with DM halos so far, only long-slit *Hubble Space Telescope* (*HST*) stellar kinematical data are available (Shen & Gebhardt 2010; Jardel et al. 2011; Schulze & Gebhardt 2011). Such data—due to the limited spatial coverage—do not fully constrain the distribution of central stellar orbits. Up to now, only three core ellipticals (Gebhardt et al. 2011; McConnell et al. 2012) have reliable measurements of the central orbital structure using both DM halos and two-dimensional (2D) kinematic data. Similar measurements for power-law, non-core elliptical galaxies are yet missing.

Here, we present a coherent analysis of the central orbital structure in 11 massive elliptical galaxies. All of our galaxies have high-resolution, adaptive optics-assisted, integral field (IFU) stellar kinematical data obtained with SINFONI at the European Southern Observatory Very Large Telescope (ESO-VLT). We use state-of-the-art axisymmetric orbit superposition models (Schwarzschild 1979) that include the effects of a central SMBH, stars, and a DM halo. Six of the galaxies are core galaxies, while five do not have detectable cores at the resolution limit of *HST* (Rusli et al. 2013b, 2013a). We compare the orbit distributions in both types of galaxies against each other and against predictions from core-formation models.

The paper is organized as follows. In Section 2, we present an overview of the galaxy sample, observations, and dynamical models. Anisotropies are described and compared with previous modeling results in Section 3. In Section 4, we compare our results quantitatively with core-formation models. The paper is summarized in Section 5.

2. OBSERVATIONS AND MODELING

Our galaxy sample is based on the set of high velocity-dispersion ellipticals in Rusli et al. (2013b) where we study the influence of DM halos on dynamical black hole mass measurements. Details of the photometric and kinematical data, the data reduction, and our modeling technique are presented therein. We observed the center of each galaxy with SINFONI at the ESO-VLT. These very high spatial resolution data guarantee that the sphere of influence of the central black hole is well resolved (Table 1). We combined these data with kinematical observations on larger scales, typically out to about the half-light radius of each galaxy. Extended spatial coverage with kinematical data is essential to constrain the distribution of stellar orbits, in particular to constrain the amount of stars on radially extended orbits. One galaxy (NGC 5516) out of the original 10-galaxy sample is omitted here since its kinematical data reach only out to $r_{\rm max} \lesssim 12\, r_b$ and the orbital structure in the core is less constrained than in the other galaxies ($r_{\rm max} > 20\, r_b$). To this sample of nine galaxies, we add two additional high-σ galaxies that we also observed with SINFONI: NGC 307 and NGC 1332. The data for NGC 1332 were already published in Rusli et al. (2011); the new data for NGC 307 are described in P. Erwin et al. (in preparation). Both new galaxies have been analyzed following the same data reduction/modeling scheme as described in Rusli et al. (2013b). To constrain the spatial distribution of the stars, we use a combination of *HST* images, ground-based images, and our SINFONI data (Rusli et al. 2013b).

Table 1
Summary of the Galaxy Sample

Galaxy	r_b (″)	$r_{\rm soi}$ (″)	FWHM (″)	$M_\bullet$ ($10^9\, M_\odot$)	$M_{\rm def}$ ($M_\bullet$)	σ_e (km s^{-1})
NGC 1407	2.0	2.0	0.19	4.5	0.96	276.1
NGC 1550	1.2	0.7	0.17	3.7	2.95	270.1
NGC 3091	0.6	0.6	0.17	3.6	4.36	297.2
NGC 4472	1.8	1.5	0.47	2.5	1.46	300.2
NGC 5328	0.9	0.7	0.14	4.7	5.70	332.9
NGC 7619	0.5	0.4	0.18	2.5	5.40	292.2
NGC 1374	···	0.8	0.15	0.6	···	166.8
NGC 4751	···	0.4	0.22	1.4	···	355.4
NGC 6861	···	0.4	0.38	2.0	···	388.8
NGC 307	···	0.2	0.17	0.6	···	201.4
NGC 1332	···	0.4	0.14	1.4	···	292.4

Notes. Core radii r_b and mass deficits $M_{\rm def}$ are from Rusli et al. (2013a). Black hole masses $M_\bullet$, sphere-of-influence radii $r_{\rm soi}$, the spatial resolution of the kinematic data, and the effective velocity dispersion σ_e are from Rusli et al. (2013b), except for the new results for NGC 307 and NGC 1332.

Six out of the eleven galaxies are core galaxies, while five do not have a detectable core at the limit of *HST* resolution (Rusli et al. 2013a). Cores in the observed galaxies were identified and measured using core-Sérsic model (Graham et al. 2003; Trujillo et al. 2004) fits to surface brightness profiles that extend out to large radii, typically more than twice the half-light radius of the galaxy (Rusli et al. 2013a). A summary of the relevant galaxy properties is given in Table 1.

2.1. Schwarzschild Modeling

The population of stellar orbits is determined by fitting Schwarzschild orbit-superposition models to these data. In our models, we assume the mass density ρ of the galaxies to be described by

$$\rho(r) = M_\bullet \times \delta(r) + \Upsilon \times \nu(r) + \rho_{\rm DM}(r), \qquad (1)$$

where $M_\bullet$ is the mass of the central SMBH, Υ is the stellar mass-to-light (M/L) ratio, and ν denotes the deprojected galaxy luminosity density. The DM density $\rho_{\rm DM}$ is modeled by a logarithmic halo, which is constrained by two parameters that are included in the fit.[3] Taking into account the effect of a DM halo is essential to derive unbiased black hole masses (Gebhardt & Thomas 2009; Rusli et al. 2013b) and, as we will show in Section 3.4, to derive an unbiased orbit distribution.

To determine the best-fitting mass models, we proceed in two steps. We first omit the central high-resolution SINFONI data and only vary Υ and the DM density $\rho_{\rm DM}$. From this first set of models, we determine $\rho_{\rm DM}(\Upsilon)$, the best-fitting DM density distribution as a function of Υ. For the final set of models, we include the central kinematical constraints from our SINFONI observations and vary $M_\bullet$ and Υ and use the relation $\rho_{\rm DM}(\Upsilon)$ determined from the first set of models (Rusli et al. 2013b). In this way, we reduce the originally 4D parameter space to two smaller ones (3D and 2D, respectively).

In each trial potential, i.e., for each particular choice of $M_\bullet$, Υ, and $\rho_{\rm DM}$, we compute an orbit library containing about 25,000 representative stellar orbits. Half of these orbits have positive angular momentum L_z along the rotation axis; the rest have their L_z flipped in the opposite direction. The contribution of each orbit to the best-fit model in the actual potential, the so-called orbital occupation number or weight, is determined by the maximization of

$$S - \alpha\chi^2, \tag{2}$$

subject to the constraints imposed by the deprojected galaxy luminosity density ν. In Equation (2), S denotes the Boltzmann entropy and χ^2 quantifies the deviations between the observed line-of-sight velocity distributions and the model. The entropy maximization and χ^2 minimization is done iteratively for $\sim$30 different values of the regularization parameter α. We start with $\alpha = 0$ and stop when an increase in α no longer reduces χ^2. Models with different α reproduce the density constraints equally well but differ in their internal orbital structure: at $\alpha = 0$, the entropy is maximized, while for larger α, the orbital weights are adjusted more to fit the model to the kinematical observations (as good as the actual trial potential allows). The results presented in this paper are based on models with maximum α, i.e., the orbit distribution is entirely determined by the observational data. A detailed description of our implementation of the Schwarzschild method can be found in Thomas et al. (2004, 2005).

3. STELLAR ORBITS IN THE CENTERS OF MASSIVE ELLIPTICALS

Figures 1(a) and (b) show the distribution of stellar orbits in our galaxies as measured from the best-fit models. The figure shows for each galaxy the radial profile of the orbital anisotropy parameter:

$$\beta_{\rm rot} = 1 - \frac{\sigma_{\rm rot}^2}{\sigma_r^2}, \tag{3}$$

where

$$\sigma_{\rm rot}^2 = \left(\sigma_\vartheta^2 + \sigma_\varphi^2 + v_\varphi^2\right)/2 \tag{4}$$

is the light-weighted spherically averaged second velocity moment in the tangential direction and σ_r the corresponding moment in the radial direction. In Figure 1(a), the radial coordinate is scaled by the core radius r_b and only core galaxies are shown. In Figure 1(b), only the non-core galaxies are shown and the radial coordinate is scaled by the sphere-of-influence radius $r_{\rm soi} = G\,M_\bullet/\sigma_e^2$. In our core galaxies, $r_{\rm soi} \sim r_b$ (Table 1).

3.1. Homology in the Velocity Dispersion Tensor

The dynamical structure around the SMBHs in core galaxies is different from that in non-core, power-law galaxies. The central anisotropy profiles of the six core galaxies are remarkably uniform. Stellar motions inside the core radius r_b are strongly dominated by tangential orbits ($\beta_{\rm rot} < 0$), while outside r_b radial orbits quickly take over ($\beta_{\rm rot} > 0$). In fact, there is a strong homology in the anisotropy profiles: when scaled by the core radius r_b, the radial profiles of the classical anisotropy parameter $\beta_{\rm rot}(r)$ are nearly identical in core galaxies. The five galaxies without cores do not show any coherent anisotropy pattern, but instead are tangentially biased on all spatial scales.

The homogeneity of the stellar orbits is not directly enforced by the break in the light profiles. To check this, we also built maximum-entropy models (e.g., Thomas et al. 2009) for each core galaxy. These models reproduce the light profile equally well but are isotropic in the center. They do not fit the observed kinematics, however, having higher central velocity dispersions and steeper velocity dispersion gradients than observed.

3.2. Previous Anisotropy Measurements

A compilation of previous anisotropy measurements in the centers of early-type galaxies is shown in Figures 1(c) and (d). Models based on IFU data are highlighted and referenced on the left, while models fitted to long-slit data are quoted on the right. All models shown in Figure 1 include an SMBH, stars, and a DM halo.

The core-galaxy models of Schulze & Gebhardt (2011) do not show a tendency toward tangential anisotropy inside the core radius r_b: instead, all three core galaxies in their sample (NGC 3608, NGC 4291, and NGC 4649) show nearly constant and isotropic dispersion profiles (Figure 1(c)). The recent models of the two brightest cluster galaxies, NGC 3842 and NGC 7768 (McConnell et al. 2012),[4] do show increasing tangential anisotropy, as do our models. We attribute the different results to the different data that were used: Schulze & Gebhardt (2011) use long-slit *HST* data that do not fully cover the central galaxy regions and leave most stellar orbits unconstrained. In contrast, the study of McConnell et al. (2012) and ours are based on IFU spectroscopic data in the center that provide full spatial coverage and the most complete constraints on stellar orbits. This indicates that IFU data are important for understanding the central orbital structure in core galaxies. However, we note that the latest model of M87 by Gebhardt et al. (2011) is based on IFU data as well. It shows tangential anisotropy only inside $r \lesssim 0.2\,r_b$. A direct comparison to our work is hampered by the fact that Gebhardt et al. (2011) do not fit a stellar M/L ratio but use the dynamical stellar M/L from Murphy et al. (2011), which was determined from kinematical data with lower central resolution. In addition to this difference in the modeling approach, the velocity dispersion profile of M87 rises steeply inside the core region, while our core galaxies have

[3] Our models are axisymmetric, i.e., the mass density is assumed to vary as a function of radius and a polar angle. For the sake of compactness, we omitted the angular dependence in Equation (1).

[4] For our comparison, we leave out two of the four galaxies from McConnell et al. (2012): NGC 2832, because only an upper limit for the mass of the central SMBH was derived, and NGC 4889, because its kinematical data reach only out to $r \lesssim 13\,r_b$.

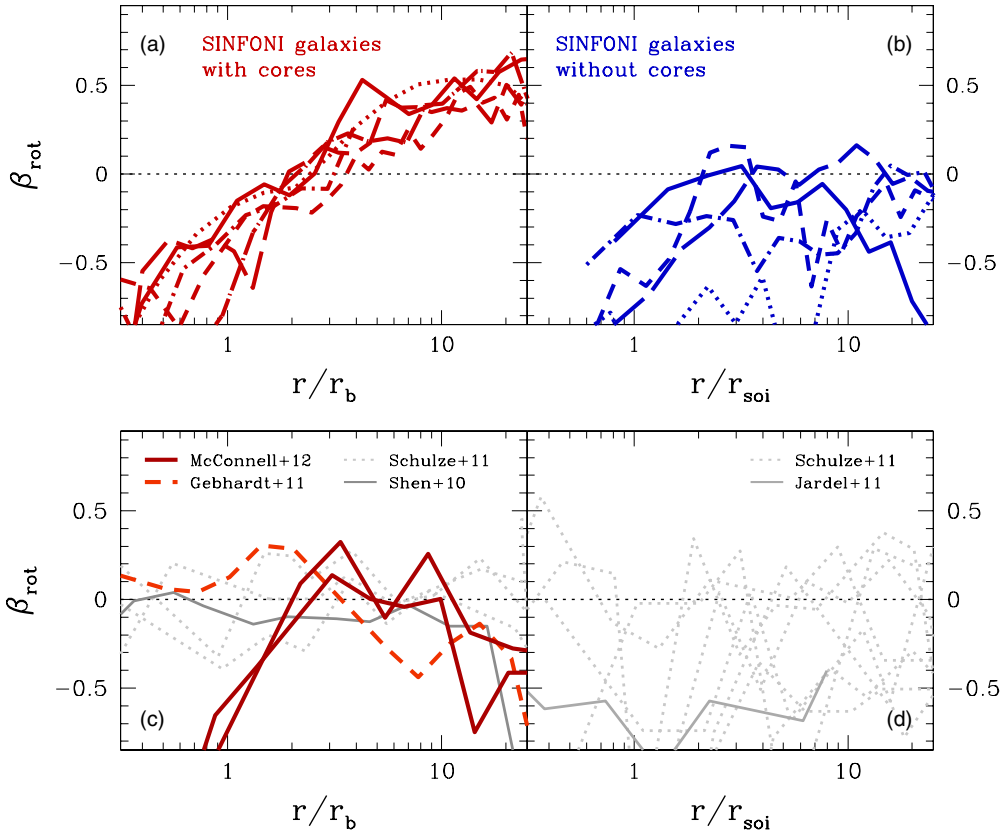

Figure 1. Central anisotropy profiles β_{rot} of early-type galaxies from models including a central SMBH, stars, and a DM halo. Top: SINFONI galaxies with cores (panel (a); radii are scaled by the core radius r_b) and SINFONI galaxies without cores (panel (b); radii are scaled by the sphere of influence r_{soi}). Our models are based on IFU kinematics. Bottom: previous galaxy models for (c) core galaxies and (d) non-core galaxies. We use the core/non-core classification of Rusli et al. (2013a). Results based on IFU data similar to ours are highlighted (Gebhardt et al. 2011; McConnell et al. 2012). All galaxy models assume axial symmetry.

nearly constant central velocity dispersion profiles (cf. Gebhardt et al. 2011 and Rusli et al. 2013b).

The situation for power-law galaxies is less clear due to the complete lack of comparison galaxies studied based on IFU data and models similar to ours: the existing models with DM for non-core galaxies by Schulze & Gebhardt (2011) and the ones for NGC 4594 (Jardel et al. 2011) are based on long-slit data. Our β_{rot} seem slightly less negative than the ones in Figure 1(d). Whether this is due to the use of IFU versus long-slit data is unclear. The published anisotropies of Schulze & Gebhardt (2011) are along the galaxies' major axes, where the influence of v_φ on the anisotropy is largest. This could also explain their more extreme tangential anisotropies, apart from intrinsic variations in the orbital structure among non-core galaxies, in which stellar orbits seem to be populated in a less coherent manner than in core galaxies.

3.3. Core Rotation

Figure 2 shows the central orbital structure of our SINFONI galaxies, split up into the *intrinsic* velocity dispersion anisotropy:

$$\beta \equiv 1 - \frac{\sigma_{\rm tang}^2}{\sigma_r^2}, \quad (5)$$

with

$$\sigma_{\rm tang}^2 \equiv \left(\sigma_\vartheta^2 + \sigma_\varphi^2\right)/2 \quad (6)$$

(panels (a) and (b)) and the stellar rotation component (panels (c) and (d)). The six core galaxies show little to no rotation in their central regions, but all five power-law galaxies rotate with values of ∼0.5–1.5 times the local velocity dispersion $\langle\sigma\rangle$. Hence, in core galaxies, $\beta_{rot} \sim \beta$ and the similarity in the central orbital structure is due to a homology in the intrinsic velocity dispersion tensor. In power-law galaxies, $\beta_{rot} < \beta$ and a significant fraction of the tangential anisotropy ($\Delta\beta \sim 0.2$–0.4) comes from stars that carry net angular momentum. The remaining anisotropy in the velocity dispersion tensor is more similar to that of core galaxies. Yet, even after separating out the rotating component, power-law galaxies still have a slightly more tangential orbit distribution.

3.4. The Importance of Dark Matter Halos

Figure 3 is similar to Figure 1, but shows the distribution of stellar orbits from models that only include an SMBH and stars (*no* DM halo). Ignoring the contribution of DM halos in the models changes the derived orbital structure significantly. In fact, in our core-galaxy models without DM (Figure 3(a)), the homology (as seen in Figure 1(a)) disappears. In the outer parts, the omission of DM reduces the amount of stars on radial orbits, which is a reflection of the well-known mass-anisotropy degeneracy, i.e., that missing mass can be partly compensated for by a more tangential orbit distribution (e.g., Binney & Mamon 1982; Gerhard 1993).

Schulze & Gebhardt (2011) did a similar comparison between models that included an SMBH, stars, and DM and models with only an SMBH and stars. Their results change only a little when DM is included. We attribute the difference to our models, which change significantly when the effect of a DM halo is included, to the fact that Schulze & Gebhardt (2011) do not allow for as

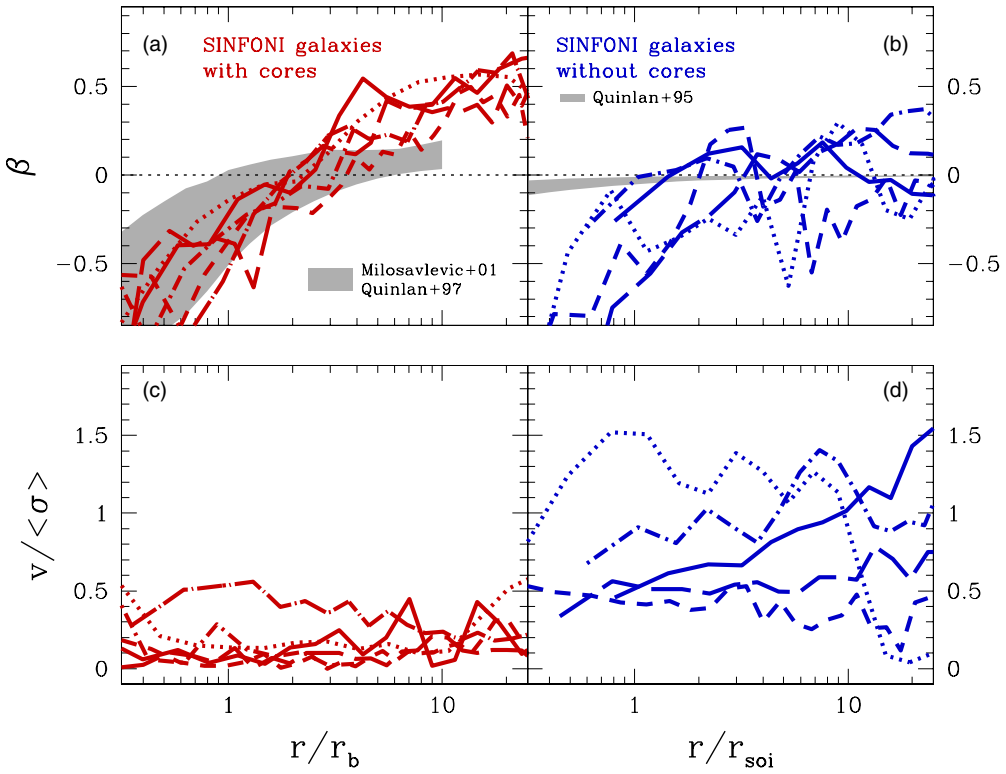

Figure 2. Top: intrinsic anisotropy profiles $\beta(r)$ of the SINFONI galaxies with (a) cores and (b) without cores. Shaded areas show predictions from numerical N-body simulations of core scouring by equal-mass binary black holes (panel (a): Quinlan & Hernquist 1997; Milosavljević & Merritt 2001) and from adiabatic SMBH growth models (panel (b): Quinlan et al. 1995). Bottom: rotation profiles along the major axis (c) in the six core galaxies and (d) the five galaxies without cores. Rotation velocities are scaled by the local velocity dispersion $\langle\sigma\rangle^2 \equiv (\sigma_r^2 + \sigma_\vartheta^2 + \sigma_\varphi^2)/3$.

much freedom in the distribution of DM as we do in our models (cf. Rusli et al. 2013b). In addition, the models of Schulze & Gebhardt (2011) rely on long-slit *HST* data, which, by their one-dimensional (1D) nature, do not fully cover the central galaxy regions and leave most of the stellar orbits unconstrained (see above). Our models presented here are instead based on IFU spectroscopic data that fully cover the galaxy centers and provide the most complete constraint on stellar orbits.

The bottom row of Figure 3 compiles previous anisotropy measurements, where those based on IFU data are again highlighted and referenced on the left, while models fitted to long-slit data are quoted on the right. Note that Gebhardt et al. (2007), Gültekin et al. (2009), and Schulze & Gebhardt (2011) used $\beta_{\rm rot}$, while all other results shown in Figures 3(c) and (d) are for β.

Core galaxy models without DM generally yield isotropic or even slightly radial orbit distributions ($\beta_{\rm rot}$, $\beta \gtrsim 0$; Figure 3(c)). According to Equation (4), $\beta_{\rm rot}$ is always lower than β. Thus, different definitions of β cannot explain why many previous studies found isotropic or slightly radial orbit distributions in core galaxies (around r_b). But the inclusion of rotation can partly explain the difference among the non-core galaxies in Figure 3(d). In any case, even with models that neglect DM halos, stellar orbits in power-law galaxies appear more strongly biased in the tangential direction than do those in core galaxies.

From Figure 1, it becomes clear that models that do include DM and an SMBH recover different orbit distributions depending on whether they are based on 2D spectroscopic data or 1D long-slit data. Without a DM halo, instead, the difference between models fit to IFU data and models fit to long-slit data is less significant (Figure 3); if anything, models fit using IFU data are slightly more radially anisotropic. This indicates that IFU data are important for the recovery of the orbital structure, because they help to constrain the gravitational potential, in particular the mass of the central SMBH, more tightly. In Rusli et al. (2013b), we find that SMBH masses change on average by a factor of $\sim$2 when including a DM halo; in a similar study, although based on 1D *HST* data, Schulze & Gebhardt (2011) find an increase in SMBH masses of only $\sim$20%.

We conclude that a reliable reconstruction of the central orbital structure requires the *combination* of IFU data and DM halos in the models; neither factor by itself is sufficient.

3.5. Uncertainties

Almost all previous works—and ours—assume axial symmetry for the studied galaxies. The only published triaxial models, for the centers of NGC 3379 and NGC 3998 (van den Bosch & de Zeeuw 2010; Walsh et al. 2012), are dominated by box orbits in the innermost regions. Box orbits do not exist in axisymmetric potentials. However, the associated radial anisotropies in the triaxial models of NGC 3379 and NGC 3998 are similar to those in other galaxies derived from similar data and assumptions about the mass profile (no DM halo). Moreover, the triaxial model of NGC 3379 is similar to the axisymmetric model of NGC 3379 by Shapiro et al. (2006) outside $r \gtrsim r_b/2$. NGC 3379 and NGC 3998 thus do not provide evidence that the assumption of axial symmetry induces a strong bias. This could be expected for the central regions where the potential is dominated by the SMBH, i.e., spherical and Keplerian. Final conclusions can only be drawn when triaxial models with a DM halo are available.

The orbit distributions derived for the centers of power-law galaxies are probably more uncertain than those for core

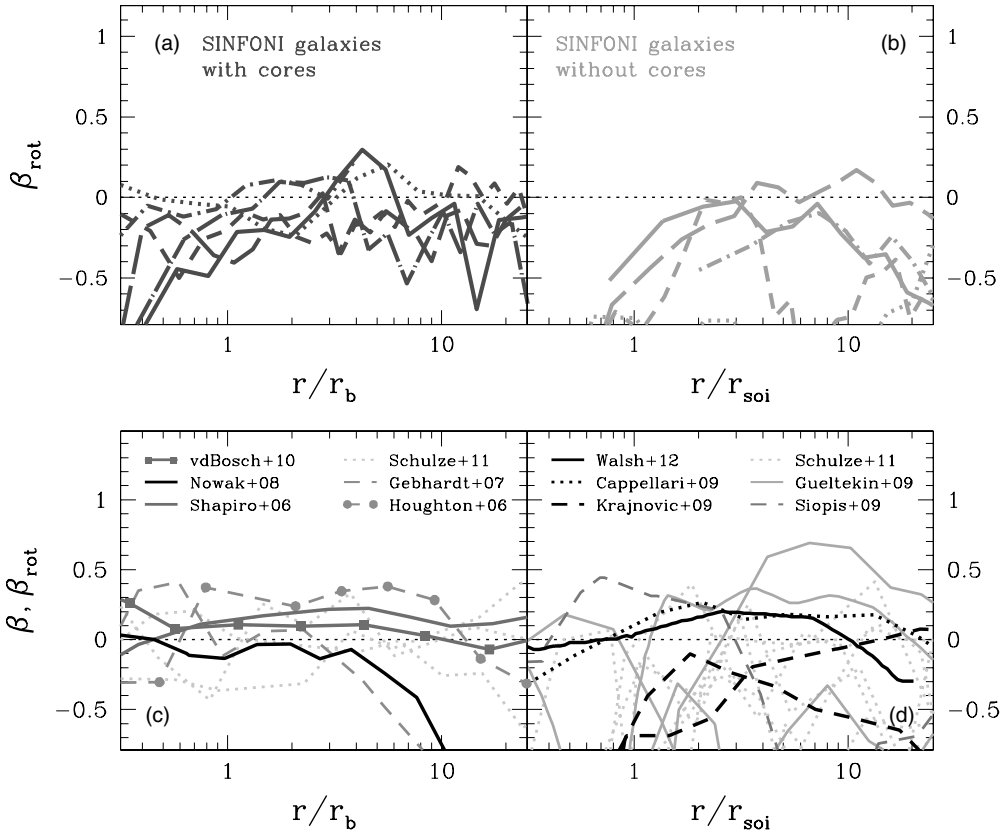

Figure 3. As in Figure 1, but for models that only include a SMBH and stars (*no* DM halo). Top: SINFONI galaxies; bottom: previous models. Results based on IFU data are again highlighted (Shapiro et al. 2006; Nowak et al. 2008; Cappellari et al. 2009; Krajnović et al. 2009; van den Bosch & de Zeeuw 2010; Walsh et al. 2012). Core galaxies are on the left ((a) and (c)); power-law galaxies are on the right ((b) and (d)). All galaxy models are axisymmetric, except for NGC 3379 and NGC 3998 (triaxial; van den Bosch & de Zeeuw 2010; Walsh et al. 2012) and NGC 1399 (spherical; Houghton et al. 2006). Note that Gebhardt et al. (2007), Gültekin et al. (2009), and Schulze & Gebhardt (2011) used β_{rot}, while all other results shown in panels (c) and (d) are for β (details in the text).

galaxies. At the innermost resolved data point, there are still orbits with pericenters at even smaller radii. These orbits are only partly constrained, by light scattered from the center to larger radii through point-spread function effects. Because power-law galaxies have brighter centers, constraints from presently unresolved spatial regions are likely to affect dynamical models more strongly than in core galaxies with their faint inner regions.

4. CORE FORMATION

The remarkable homogeneity of the orbital structure in the core galaxies and the fact that the transition from tangential to radial anisotropy is strongly correlated with the core radius r_b provide an observational link between core formation and the population of central stellar orbits. Moreover, the core formation process must be very uniform to produce the observed homology in the distribution of core stellar orbits.

4.1. Adiabatic Growth and Core Expansion

Tangential anisotropy in the core could be the result of adiabatic black hole growth (Goodman & Binney 1984). For two reasons, however, this process is unimportant for stellar orbits in core galaxies. First, the effect of adiabatic black hole growth on the orbital structure is weak and confined to the region inside r_{soi}: the shaded area in Figure 2(b) shows models of Quinlan et al. (1995). They start from an isotropic orbit distribution and initial central logarithmic density slopes of $\gamma = \{0, -1\}$. Even when the final black hole mass is up to 10% of the galaxy mass, the change in the central anisotropy remains modest ($|\Delta\beta| \leqslant 0.3$; see also Young 1980 and Goodman & Binney 1984). If adiabatic black hole growth was the main driver behind the observed anisotropy in the cores of massive ellipticals, then the orbits would be required to be highly coherent and correlated with r_{soi} already before the black hole growth. Our coreless galaxies do not provide evidence for this. Second, adiabatic black hole growth steepens the central light profile (Young 1980) and thus cannot explain the formation of cores in the first place. Core creation through dynamical friction-driven angular momentum transfer from infalling objects (Goerdt et al. 2010) and core expansion in reaction to gas ejection by an active galactic nucleus (Martizzi et al. 2012) are unlikely as well. These processes are not directly linked to the mass of the central black hole and hence cannot explain the fact that cores sizes correlate tightly with $M_\bullet$ (Rusli et al. 2013a). These processes might, however, be important for less massive, fast-rotating core galaxies (e.g., Krajnović et al. 2013).

4.2. Core Formation by Binary Black Holes

Quinlan & Hernquist (1997) studied the response of a galaxy's orbital anisotropy and its 3D density profile to a central, equal-mass black hole binary, starting from isotropic systems with various inner logarithmic density slopes. We fit core radii r_b to their simulations with black hole masses in the range $M_\bullet = (0.005\text{–}0.02)\, M_{tot}$ and initial slopes $\gamma = \{-1, -2\}$, typical for power-law ellipticals. To ensure compatibility with the core radii measured in real galaxies, the fits were performed using the (approximate) deprojection of the core-Sérsic model

given by Terzić & Graham (2005). When scaled by these core radii, the anisotropy profiles of the Quinlan & Hernquist (1997) simulations are all very similar. They define the lower boundary of the shaded region in Figure 2(a).

Milosavljević & Merritt (2001) investigated the entire merging process of two identical elliptical galaxies with initial central density slopes $\gamma = -2$ and also measured core radii from the remnant's final projected surface mass profile. Their definition of r_b (radius of maximum curvature) differs slightly from our r_b derived with core-Sérsic models, but the difference is small ($\sim$10%). The results of Milosavljević & Merritt (2001) define the upper boundary of the shaded area in Figure 2(a).

Both simulations predict a transition in the orbital structure around the core radius: inside r_b, tangential orbits dominate; outside the core, radial orbits take over. Similar anisotropy patterns have been derived in other simulations as well (Zier & Biermann 2001; Meiron & Laor 2010; Antonini & Merritt 2012).

The observed orbital structure of the core galaxies follows this prediction closely, while non-core galaxies do not exhibit the characteristic change in the orbital structure from tangential to radial anisotropy. This provides the first convincing dynamical evidence for core scouring in massive elliptical galaxies.

4.3. Mass Deficits and Merging Histories

A single binary is expected to eject about its own mass in stars from the center (Merritt 2006). Larger mass deficits can result from:

1. the cumulative effect of repeated mergers (Merritt 2006);
2. repeated core passes of the post-binary-merger black hole due to gravitational-wave recoil (Gualandris & Merritt 2008) ($M_{\rm def} \lesssim 5\,M_\bullet$);
3. multiple black hole systems that might form at high redshifts (Kulkarni & Loeb 2012) ($M_{\rm def} \lesssim 5\,M_\bullet$).

The mass deficits derived for our core galaxies are $M_{\rm def} \sim$ 1–6 $M_\bullet$ (Table 1) and, again, fit the numerical predictions well.

Most of our galaxies have mass deficits consistent with only one major merger, in agreement with their orbital anisotropy. A corresponding number of minor mergers, however, would give similar mass deficits. Studies of test-particle orbits around equal-mass as well as unequal-mass black hole binaries suggest that the central anisotropy, like the mass deficit, does not carry specific information about the merging history (Meiron & Laor 2010).

Such information could, however, be encoded in the central rotation velocities. In equal-mass merger simulations, rotation velocities similar to the local velocity dispersion are found (Milosavljević & Merritt 2001; Meiron & Laor 2013). Unequal-mass binaries likely induce less rotation through dynamical friction (Meiron & Laor 2013). Rotation velocities in our observed cores are small (Figure 2). This might favor a sequence of several minor mergers, where, if the merger orbits are random, each new merger would tend to wash out the rotation signal left over from the previous merger. The stochastic behavior of possible multiple black hole systems, formed as a consequence of successive minor mergers, might further reduce core rotation in real galaxies. Constraints from galaxy scaling relations, however, limit the mass ratios of precursor galaxies as well (Kormendy & Bender 2013). To put more quantitative constraints on the detailed formation histories of core galaxies, we need (1) numerical simulations that explore a wider range of initial conditions and (2) discussion of stellar population properties (something we plan for a forthcoming paper).

4.4. Non-core Galaxies

The five non-core galaxies of our sample are not consistent with simple models of an adiabatic black hole growth into an originally isotropic stellar distribution: the relative overpopulation of tangential orbits with stars is stronger and spread over a spatially more extended region than expected from these models.

They are, however, compatible with the idea that these galaxies form in gas-rich mergers, where any pre-existing core is "refilled" by gas that falls in during/after the merger, settles into a rotating configuration, and then forms new stars. In fact, the intrinsic anisotropy (without rotation) of non-core galaxies shows a slight tendency toward a gradient from tangential anisotropy in the center toward a more isotropic or radially dominated orbit system at $r \gtrsim r_{\rm soi}$ that is similar to the transition in core galaxies, although with significantly more scatter. This imprint in the stellar orbits could be the relic of a transient core structure that occurred at some point during the formation of these galaxies and led to a partially depleted core (although the dynamical friction on the SMBHs is much stronger in a gaseous environment and the timescale for interactions between stars and the SMBHs is correspondingly short). In this scenario, a strong rotating component would also be present, consisting of the stars that formed later, refilling the core and possibly producing the central extra light component discussed by, e.g., Côté et al. (2006), Kormendy & Bender (2009), Kormendy et al. (2009), and Kormendy & Ho (2013).

Another explanation for the central tangential orbits might be a reshaping of the stellar orbits similar to the adiabatic SMBH-growth scenario, but originating from the formation of a concentrated stellar density cusp during a dissipational merger. Quantitative predictions for the central orbital structure from numerical simulations including gas dissipation and star formation are not available yet, however.

5. SUMMARY

We analyze the central distribution of stellar orbits in 11 massive early-type galaxies, derived from orbit-based Schwarzschild models including a central SMBH, stars, and DM halos. Six of our galaxies are core galaxies; the other five have power-law centers. This is the first consistent analysis of a sample of massive core as well as non-core early-type galaxies to study the homology of stellar orbits based on homogeneous, high-resolution, IFU spectroscopic data, and state-of-the-art modeling techniques.

The comparison of previous modeling attempts using either data with less spatial coverage and/or models that lacked DM halos indicates that both 2D IFU data coverage in the center and accounting for the effects of DM are necessary for unbiased measurements of the distribution of stellar orbits.

In core galaxies, the distribution of stellar orbits shows a coherent change from mostly tangential orbits inside r_b to mostly radial orbits further out. Moreover, there is a remarkable homology: when scaled by the core radius r_b, the radial profiles of the classical anisotropy parameter $\beta(r)$ are nearly identical in core galaxies. Power-law galaxies do not take part in this homology. The scatter in the distribution of stellar orbits in these galaxies is larger, but indicates a preference of tangential orbits as well.

The orbital structure observed in the centers of core galaxies matches the predictions of black hole binary models. They do not match predictions of adiabatic growth models, although both models favor tangential orbits in the center. The difference is (1) in the magnitude of the tangential bias and (2) in the change of the orbit distribution with radius, in particular that radial orbits dominate outside the core in SMBH-binary models. Our observations provide the first convincing direct dynamical evidence for core scouring in massive elliptical galaxies.

Some of the data used in this paper were obtained using SINFONI at the Very Large Telescope (VLT) and from the Mikulski Archive for Space Telescopes (MAST). The VLT is operated by the European Southern Observatory on Cerro Paranal in the Atacama desert of northern Chile. STScI is operated by the Association of Universities for Research in Astronomy, Inc., under NASA contract NAS5-26555. This paper also includes data taken at The McDonald Observatory of The University of Texas at Austin.

R.P.S. and R.B. acknowledge support from the DFG Cluster of Excellence Origin and Structure of the Universe. P.E. was supported by the Deutsche Forschungsgemeinschaft through the Priority Programme 1177 "Galaxy Evolution."

Finally, this work has made use of the NASA/IPAC Extragalactic Database (NED), which is operated by the Jet Propulsion Laboratory, California Institute of Technology, under contract with the National Aeronautics and Space Administration.

REFERENCES

Antonini, F., & Merritt, D. 2012, ApJ, 745, 83
Begelman, M. C., Blandford, R. D., & Rees, M. J. 1980, Natur, 287, 307
Binney, J., & Mamon, G. A. 1982, MNRAS, 200, 361
Boylan-Kolchin, M., & Ma, C.-P. 2004, MNRAS, 349, 1117
Caon, N., Capaccioli, M., & D'Onofrio, M. 1993, MNRAS, 265, 1013
Cappellari, M., Neumayer, N., Reunanen, J., et al. 2009, MNRAS, 394, 660
Côté, P., Piatek, S., Ferrarese, L., et al. 2006, ApJS, 165, 57
Cretton, N., & van den Bosch, F. C. 1999, ApJ, 514, 704
Faber, S. M., Tremaine, S., Ajhar, E. A., et al. 1997, AJ, 114, 1771
Fulton, E., & Barnes, J. E. 2001, Ap&SS, 276, 851
Gebhardt, K., Adams, J., Richstone, D., et al. 2011, ApJ, 729, 119
Gebhardt, K., Bender, R., Bower, G., et al. 2000, ApJL, 539, L13
Gebhardt, K., Lauer, T. R., Pinkney, J., et al. 2007, ApJ, 671, 1321
Gebhardt, K., Richstone, D., Tremaine, S., et al. 2003, ApJ, 583, 92
Gebhardt, K., & Thomas, J. 2009, ApJ, 700, 1690
Gerhard, O. E. 1993, MNRAS, 265, 213
Goerdt, T., Moore, B., Read, J. I., & Stadel, J. 2010, ApJ, 725, 1707
Goodman, J., & Binney, J. 1984, MNRAS, 207, 511
Graham, A. W. 2004, ApJL, 613, L33
Graham, A. W., Erwin, P., Trujillo, I., & Asensio Ramos, A. 2003, AJ, 125, 2951
Gualandris, A., & Merritt, D. 2008, ApJ, 678, 780
Gültekin, K., Richstone, D. O., Gebhardt, K., et al. 2009, ApJ, 695, 1577
Hopkins, P. F., & Hernquist, L. 2010, MNRAS, 407, 447
Houghton, R. C. W., Magorrian, J., Sarzi, M., et al. 2006, MNRAS, 367, 2
Jardel, J. R., Gebhardt, K., Shen, J., et al. 2011, ApJ, 739, 21
Kormendy, J., & Bender, R. 1996, ApJL, 464, L119
Kormendy, J., & Bender, R. 2009, ApJL, 691, L142
Kormendy, J., & Bender, R. 2013, ApJL, 769, L5
Kormendy, J., Fisher, D. B., Cornell, M. E., & Bender, R. 2009, ApJS, 182, 216
Kormendy, J., & Ho, L. C. 2013, ARA&A, 51, 511
Krajnović, D., Karick, A. M., Davies, R. L., et al. 2013, MNRAS, 433, 2812
Krajnović, D., McDermid, R. M., Cappellari, M., & Davies, R. L. 2009, MNRAS, 399, 1839
Kulkarni, G., & Loeb, A. 2012, MNRAS, 422, 1306
Martizzi, D., Teyssier, R., & Moore, B. 2012, MNRAS, 420, 2859
McConnell, N. J., Ma, C.-P., Murphy, J. D., et al. 2012, ApJ, 756, 179
Meiron, Y., & Laor, A. 2010, MNRAS, 407, 1497
Meiron, Y., & Laor, A. 2013, MNRAS, 433, 2502
Merritt, D. 2006, ApJ, 648, 976
Milosavljević, M., & Merritt, D. 2001, ApJ, 563, 34
Murphy, J. D., Gebhardt, K., & Adams, J. J. 2011, ApJ, 729, 129
Nowak, N., Saglia, R. P., Thomas, J., et al. 2008, MNRAS, 391, 1629
Quinlan, G. D., & Hernquist, L. 1997, NewA, 2, 533
Quinlan, G. D., Hernquist, L., & Sigurdsson, S. 1995, ApJ, 440, 554
Rusli, S. P., Erwin, P., Saglia, R. P., et al. 2013a, AJ, 146, 160
Rusli, S. P., Thomas, J., Erwin, P., et al. 2011, MNRAS, 410, 1223
Rusli, S. P., Thomas, J., Saglia, R. P., et al. 2013b, AJ, 146, 45
Schulze, A., & Gebhardt, K. 2011, ApJ, 729, 21
Schwarzschild, M. 1979, ApJ, 232, 236
Sérsic, J. L. 1963, BAAA, 6, 41
Shapiro, K. L., Cappellari, M., de Zeeuw, T., et al. 2006, MNRAS, 370, 559
Shen, J., & Gebhardt, K. 2010, ApJ, 711, 484
Siopis, C., Gebhardt, K., Lauer, T. R., et al. 2009, ApJ, 693, 946
Terzić, B., & Graham, A. W. 2005, MNRAS, 362, 197
Thomas, J., Jesseit, R., Saglia, R. P., et al. 2009, MNRAS, 393, 641
Thomas, J., Saglia, R. P., Bender, R., et al. 2004, MNRAS, 353, 391
Thomas, J., Saglia, R. P., Bender, R., et al. 2005, MNRAS, 360, 1355
Trujillo, I., Erwin, P., Asensio Ramos, A., & Graham, A. W. 2004, AJ, 127, 1917
van den Bosch, R. C. E., & de Zeeuw, P. T. 2010, MNRAS, 401, 1770
Verolme, E. K., Cappellari, M., Copin, Y., et al. 2002, MNRAS, 335, 517
Walsh, J. L., van den Bosch, R. C. E., Barth, A. J., & Sarzi, M. 2012, ApJ, 753, 79
Young, P. 1980, ApJ, 242, 1232
Zier, C., & Biermann, P. L. 2001, A&A, 377, 23